processes

MDPI

Article

Experimental Study on Yield Strength Variation Law of Casing Materials under Alternating Thermal–Mechanical Coupling Loads

Caihong Lu [1,2,*], Shangyu Yang [1], Jianjun Wang [1], Lihong Han [1], Xinbo Zhao [3,*], Yue Qi [2,4] and Hui Zhang [2]

[1] State Key Laboratory of Oil and Gas Equipment, Tubular Goods Research Institute of CNPC, Xi'an 710077, China; yangshangyu@cnpc.com.cn (S.Y.); wangjianjun003@cnpc.com.cn (J.W.); hanlihong@cnpc.com.cn (L.H.)
[2] College of Petroleum Engineering, China University of Petroleum-Beijing, Beijing 102249, China; qiyue@cnpc.com.cn (Y.Q.); zhanghui3702@163.com (H.Z.)
[3] School of Science, Qingdao University of Technology, Qingdao 266520, China
[4] Drilling Engineering Technology Research Institute of Daqing Drilling Engineering Company, Daqing 163413, China
* Correspondence: lucaihong@cnpc.com.cn (C.L.); zxbups@163.com (X.Z.); Tel.: +86-029-81887980 (C.L.)

Abstract: Unconventional oil and gas reservoirs, characterized by low porosity and permeability, often require multistage fracturing techniques for development. The high-pressure fracturing fluids with large volumes can easily cause alternating changes in both temperature and pressure within the casing. Using a theoretical model and field data from hydraulic fracturing operations, this paper calculated the alternating ranges of axial loads and temperatures in the reservoir section. Based on the calculation results, the temperature–load alternating coupling test of the P110 casing was carried out, and the tensile test was performed to analyze the yield strength variation law of the casing material. The results indicate that the yield strength, ultimate strength, and elastic modulus of casing materials are decreased under alternating thermal–mechanical coupling conditions. As the number of alternating cycles increases, there is an initial rapid decrease followed by a slower declining trend. Moreover, the tension–tension (T–T) cycles induce greater reductions in yield strength and ultimate strength than tension–compression (T–C) cycles. Meanwhile, under the same axial load condition, the higher the circulating temperature, the more significant the reduction in yield strength and ultimate strength. In essence, this is the result of the coupling effect of low-cycle fatigue and temperature aging. Finally, based on the experimental data, a yield strength prediction model of the P110 casing under the alternating thermal–mechanical coupling condition was established. The research results provide theoretical guidance for the safe design and material selection of a casing string under multistage volumetric fracturing conditions of shale gas exploration.

Keywords: unconventional oil and gas development; multistage fracturing; alternating thermal–mechanical coupling condition; yield strength; P110 casing

check for updates

Citation: Lu, C.; Yang, S.; Wang, J.; Han, L.; Zhao, X.; Qi, Y.; Zhang, H. Experimental Study on Yield Strength Variation Law of Casing Materials under Alternating Thermal–Mechanical Coupling Loads. *Processes* **2024**, *12*, 708. https://doi.org/10.3390/pr12040708

Academic Editor: Kian Jon Chua

Received: 26 January 2024
Revised: 7 March 2024
Accepted: 19 March 2024
Published: 30 March 2024

1. Introduction

The unconventional oil and gas reservoirs typically feature low porosity and permeability. To efficiently develop these reservoirs, horizontal well drilling combined with multistage hydraulic fracturing technology is an essential and cost-effective method [1,2]. However, the large fluid volumes, high pumping pressures, and multistage fracturing operations put the downhole casings under demanding conditions [3]. And according to statistics [4], among 3852 fracturing stages conducted in 145 wells within the Changning shale gas block, 59 wells experienced casing deformation, resulting in a casing deformation rate of 40.7%. Similarly, in the Weiyuan block, among 38 shale gas fracturing wells, 16 experienced casing deformation, resulting in a casing deformation rate of 42%. The

logging data results of casing radial deformation are shown in Figure 1. The results indicate that the casing is subjected to excessive non-uniform extruding and shearing loads during multistage volumetric fracture, and the lower yield strength of the casing is also one of the reasons for casing deformation. The multistage volumetric fracture process provides a temperature and pressure alternating coupling environment, which significantly increases the possibility of a yield strength reduction in the casing [5,6].

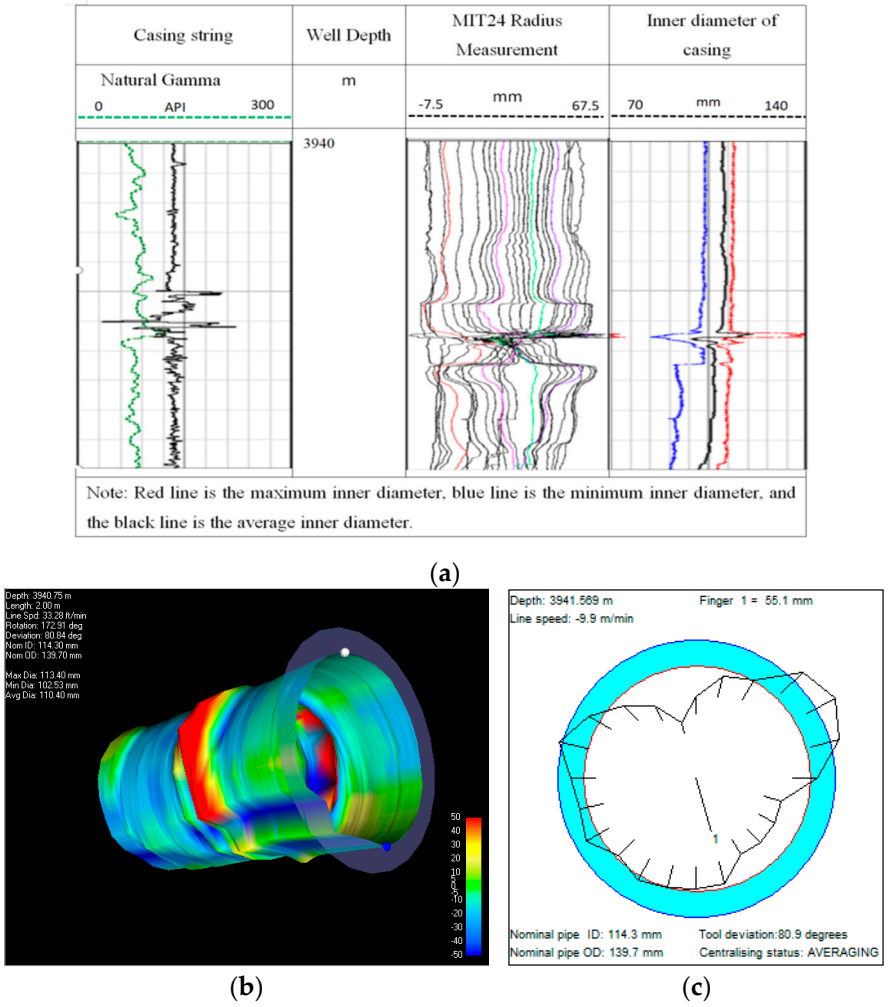

Figure 1. The logging map of Φ139.7 casing deformation at depth 3941–3942 m in shale gas well. (**a**) MIT24 logging curve. (**b**) 3D diagram. (**c**) Section diagram.

The influence of alternating load on the strength of pipe string was studied. Khan [7] performed a comprehensive three-dimensional nonlinear dynamic analysis of risers in the time domain using the finite element solver ABAQUS/Aqua. They detailed the interaction between fracture and plastic collapse based on a bilinear fatigue model and failure criteria associated with crack propagation. Additionally, Liu Xiuquan [8] introduced fracture mechanics methods to establish a fatigue failure model for deep water drilling risers. Xiao Na [9] investigated the high-cycle fatigue behavior of vacuum-carburized 20Cr2Ni4 steel at three different depths of carburization layers through rotating bending fatigue tests. Their findings revealed a trend of decreasing fatigue strength with rising effective casing depth. Furthermore, Teodoriu. C [10] conducted experiments on casing failure under alternating axial pressure loads, proving that casings are more susceptible to deformation failure under alternating loading conditions compared to static loads.

On the other hand, the primary focus of the impact of alternating temperatures on casings has been on the steam-assisted gravity drainage (SAGD) technique in heavy oil

fields [11]. Maruyama [12] and Hsu [13] conducted statistical analyses of the relationship between the number of damaged casings and the cycles of steam injection. They found a certain correlation between casing damage and the occurrences of thermal cyclic alternating loads and the number of SAGD cycles. Placido J.C.R. [14] simulated and recorded the stress on casings subjected to multiple cycles of thermal alternating loads through experimental studies. Their conclusion was that after a single cycle of heating and cooling, casings primarily experience residual tensile stress, which increases with the strength of the casing steel grade. Kasier T. [15] studied the thermo-mechanical behavior of casing materials under thermal alternating loads using static material property tests. Gan Quan [16], through establishing a 2D thermal–structural coupling finite element model of casing–cement sheath-formation, analyzed the stress changes in the casing and cement sheath during steam injection–soaking–production processes. Yin [17] investigated the influence of alternating thermal stresses during the hydraulic fracturing process on casings. The results indicated that variations in annular pressure caused by cold fracturing fluids increase the risk of casing deformation. Yin Hu [18] extensively examined the construction processes and conditions of hydraulic fracturing in horizontal shale gas wells. They pointed out that temperature has a more pronounced effect on the collapsing strength.

Numerous scholars both domestically and internationally have studied the casing deformation mechanisms during multistage fracturing processes. For instance, Tian Zhonglan [19] detected the mechanism of casing damage under various coupled conditions such as temperature effects, axial pressure, and bending. She highlighted that a significant drop in temperature occurs within the confined fluid in the chamber, resulting in a marked reduction in volume and rapid pressure decline during the fracturing stage. Consequently, casing deformation is due to pressure imbalances both inside and outside the casing. Liu Zhengchun [20] and An Fengchen [21] explored the effects of cyclic stress on casing damage. Wu Rui [22] utilized numerical analysis techniques to develop a predictive fatigue model for the fatigue life of straight wellbore columns. Mou Yisheng [23] delved into casing fatigue casing mechanisms of high-temperature and high-pressure wellbore. Wang Jianjun and Lu Caihong [24,25] have noticed that temperature and load alternating changes cause a strength reduction in the casing in gas storage injection and production wells. Shangyu Yang and Caihong Lu et al. have drafted and published China's national standard and the test group standard for the casing strength evaluation method under temperature–load alternating coupling conditions during the multistage volumetric fracturing of shale gas exploration [26,27].

However, there are few studies that test the alternating thermal–mechanical coupling condition and the residual strength prediction method of a high-grade casing under the environment of the multistage volumetric fracturing of shale gas exploration. In this paper, the thermal–mechanical coupling alternating test device of a casing was set up independently. Then the temperature and load alternating range are calculated theoretically according to the multistage volumetric fracturing condition of a typical oilfield, and the test temperature, load, and other parameters are determined. Finally, a prediction model of the residual strength of the casing after different thermal–mechanical cycles is established to provide theoretical guidance for the safe design and material selection of the casing string under multistage volumetric fracturing conditions of shale gas exploration.

2. Materials and Methods

2.1. Materials

The P110 casing material is used in this experiment, of which main chemical composition (mass fraction, %) is Fe-0.25C-0.3Si-0.5Mn-1.0Cr-0.018Mo-0.009P-0.002S. The tensile samples are machined along the axis of the casing (shown in Figure 2a), according to drawings shown in Figure 2b, and processed by grinding and polishing equipment, as shown in Figure 2c.

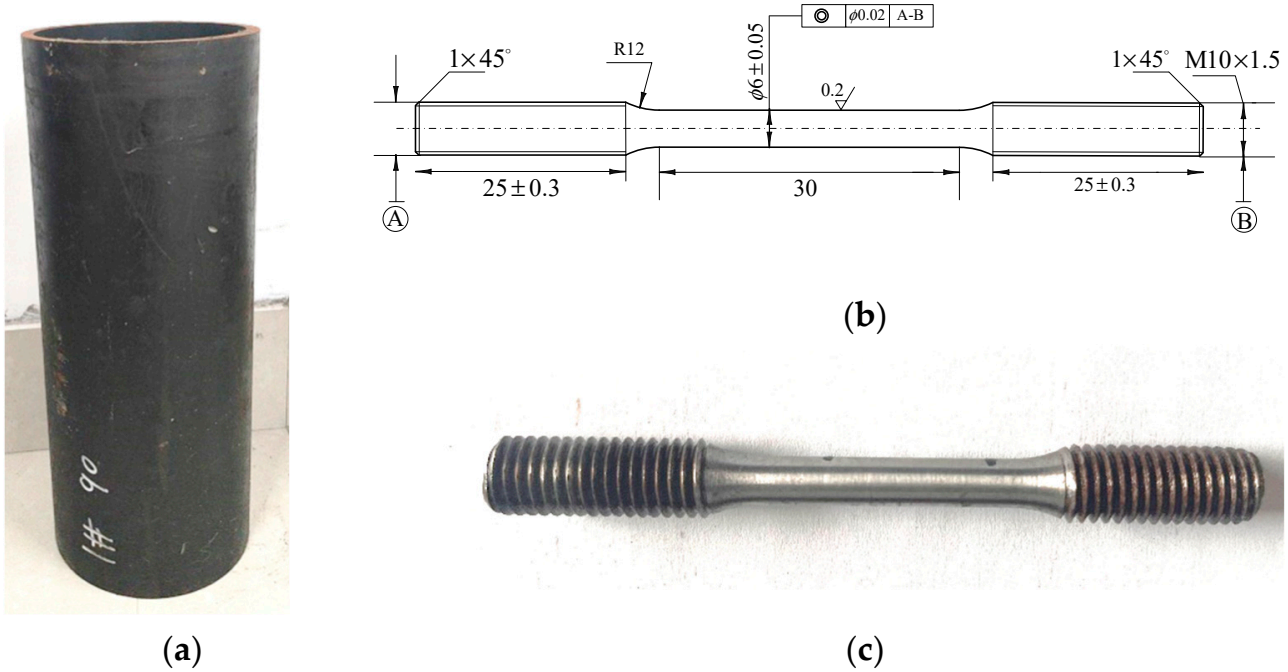

Figure 2. Experimental materials and specimens. (**a**) Physical casing. (**b**) Processing sample drawings. (**c**) Sample after processing.

2.2. Experiment Method

The experimental system shown in Figure 3 is mainly divided into two modules: One module provides axial tensile and compressive loads at the end of the specimen by MTS fatigue testing equipment; The other one is the temperature control module, which provides cooling function by air conditioning and blower, and heating function by environmental chamber and electric heating wire. The heating and cooling processes are controlled simultaneously by a time-controlled switch and a temperature-controlled switch. The test loading flow chart is shown in Figure 4, and the main performance parameters of equipment are shown in Table 1.

Table 1. Main performance parameters of experimental equipment.

Device Name	Manufacturer	Type	Country	Performance Parameter	Value
MTS fatigue testing machine	MTS systems corporation	322.31	Eden Prairie, MN, USA	Max. tensile force/kN Loading frequency/Hz	250 <100
Environmental chamber	MTS systems corporation	651	Eden Prairie, MN, USA	Heating rate/°C/min Max. temperature/°C	30 150
Vortex air pump	Shanghai Fanghong Electromechanical Equipment Co., Ltd.	HG-1500	Shanghai, China	Max. flow/m^3/h	250
Electrical cabinet air conditioning	Shanghai Xunyu Industrial Co., Ltd.	EA-3200	Shanghai, China	Cooling power/W Temperature range/°C	3200 25–35
Contact relay	Chint Group Co., Ltd.	Cjx2-3210	Wenzhou, China	Max. current/A	32
Timer switch controller	Chint Group Co., Ltd.	DH48S-S	Wenzhou, China	Number of time controls	2

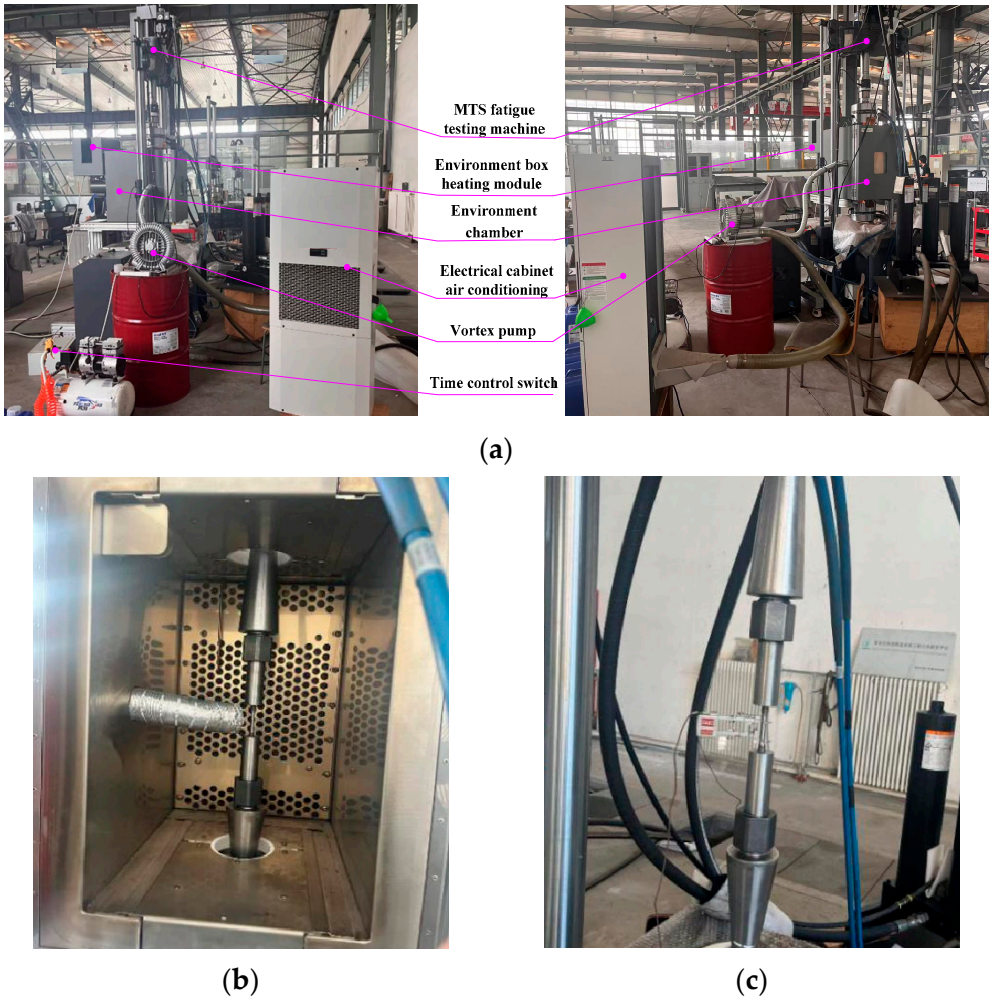

Figure 3. Testing equipment and specimen installation. (**a**) Diagram of alternating thermal–mechanical coupling test device. (**b**) Sample in the environmental chamber. (**c**) Tensile test at room temperature.

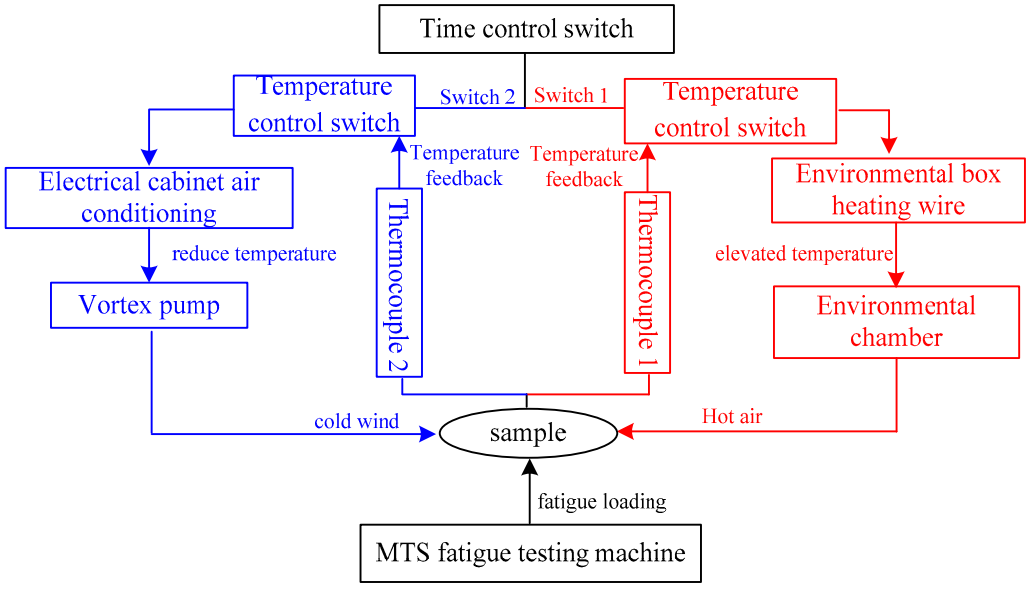

Figure 4. Control flowchart of alternating thermal–mechanical coupling loads.

According to Figure 4, firstly, the time control switch 1 and the temperature control switch 1 are turned on to start the heating module. The ambient chamber is heated by the electric heating wire to raise the temperature of sample. Meanwhile, the axial fatigue load cycle test module is started. When the temperature of sample rises to the set value, both time control switch 1 and the temperature control switch 1 are turned off, and then time control switch 2 and the temperature control switch 2 are turned on. The air conditioning and the vortex pump blow the cooling air into the ambient chamber to cool down the sample. When the sample is cooled down to room temperature, turn off the time control switch 2 and the temperature control switch 2; meanwhile, the time control switch 1 and the temperature control switch 1 are turned on to start the heating procedure. The frequency of heating and cooling cycles is once every 30 min until the MTS fatigue tests finish.

The coupling axial load cyclic test parameters are determined by the following theoretical calculations.

2.3. Determination of the Coupling Axial Cycle Loading Test Parameters

2.3.1. Determination of Casing Axial Force Load during Hydraulic Fracturing

According to experimental simulations, axial stress mainly consists of four parts:

$$\sigma_{oe} = \sigma_c + \sigma_M + \sigma_z + \sigma_H \tag{1}$$

where σ_{oe} is the axial stress, MPa; σ_c is the hydrostatic pressure from the cement acting as a compressive stress on the casing, MPa; σ_M is the tensile stress caused by self-weight, MPa; σ_z is the axial stress induced by bending, MPa; and σ_H is the axial stress induced by hydraulic fracturing, MPa.

The calculation formula for the compressive stress generated by the buoyancy of the casing string in cementing cement on the casing is as follows:

$$\sigma_c = 10^{-4} \times (-\gamma_1 L - \gamma_2 (L - l))s \tag{2}$$

where γ_1 is the density of drilling mud, kg/m^3; γ_2 is the density of cement slurry, kg/m^3; L is the length of the casing, m; l is the depth of cement sheath, m; and s is the cross-sectional area of the casing, m^2.

The calculation formula for tensile stress caused by self-weight is as follows:

$$\sigma_M = \frac{10 \times q(L - h)}{s} \tag{3}$$

where q is the weight of the casing per unit length, kg/m; and h is the depth of the calculation point, m.

The calculation formula for axial stress caused by bending is as follows:

$$\sigma_z = \pm 5.8178 \times 10^{-4} Ecr \tag{4}$$

where E is the elastic modulus, MPa; c is the bending curvature of the pipe body, 1; r is the radial coordinate, 1; and the value range is $0.5d \leq r \leq 0.5D$.

The axial stress induced by hydraulic fracturing can be calculated using the Lamé solution from elasticity theory. Assuming the casing–cement–formation composite model is axially symmetric and follows a plane strain model, the stress field expression for each layer of the structure is as follows:

$$\begin{cases} \sigma_r = -\frac{\frac{b^2}{r^2} - 1}{\frac{b^2}{a^2} - 1} q_a - \frac{1 - \frac{a^2}{r^2}}{1 - \frac{a^2}{b^2}} q_b \\ \sigma_\varphi = \frac{\frac{b^2}{r^2} + 1}{\frac{b^2}{a^2} - 1} q_a - \frac{1 + \frac{a^2}{r^2}}{1 - \frac{a^2}{b^2}} q_b \end{cases} \tag{5}$$

where σ_r and σ_φ are the radial stress and hoop stress, respectively, MPa; q_a is the internal pressure in the thick-walled cylinder, MPa; q_b is the external pressure on the thick-walled cylinder, MPa; a is the inner radius of the thick-walled cylinder, m; b is the outer radius of the thick-walled cylinder, m; and r is the casing radius, m.

The expression for radial displacement can be derived from the physical and geometric equations under plane strain conditions:

$$u_r = r \cdot \varepsilon_\varphi = r \cdot \frac{1-\mu^2}{E}\left(\sigma_\varphi - \frac{\mu}{1-\mu}\sigma_r\right) \tag{6}$$

Here, μ is Poisson's ratio of casing, 1.

According to the equality of radial displacements at the first and second bonding interfaces of the formation, cement sheath, and casing, the radial pressure at the outer layer of the casing can be determined. Consequently, the radial and hoop stresses of the casing can be obtained according to Equation (5). And then, employing the generalized Hooke's law and assuming a plane strain model, the additional axial stress generated in the casing during hydraulic fracturing can be calculated as follows:

$$\sigma_H = \mu(\sigma_r + \sigma_\varphi) \tag{7}$$

2.3.2. Calculation of Wellbore Temperature Field during Hydraulic Fracturing

In the multistage volume fracturing process, temperature changes adhere to the principle of energy conservation. For any arbitrary unit, at a specific moment, the energy conservation relationship can be described as follows: the heat entering the unit from various directions and in various forms, minus the heat leaving the unit through different methods, plus the instantaneous power of internal heat sources in the unit, equals the increased heat stored within the unit.

Considering the injection wellbore as the subject of analysis, assume a fluid with a volume flow rate Q flowing downward in the wellbore. At a distance z from the wellhead, based on the energy conservation equation, the governing equation for the temperature change of the fluid in the wellbore can be established:

$$-\rho_0 C_0 Q\frac{\partial T_0}{\partial z} + \frac{2\pi r_0(T_1 - T_0)}{R_0} + \frac{f\rho_0 v^2 Q}{4r_0} = \rho_0 C_0 \pi r_0^2 \frac{\partial T_0}{\partial \tau} \tag{8}$$

Here, ρ_0 and C_0 are the density and specific heat capacity at constant pressure of the fracturing fluid, respectively, kg/m^3 kJ/(kg·°C); T_0 and T_1 are the temperature inside the casing and at the casing wall, respectively, °C; Q denotes the volume flow rate of the fluid, m^3/h; $R_0 = r_0 - r_1/2\lambda_1$, where λ_1 is the fluid's heat transfer coefficient, kJ/(m·min·°C); f is the friction coefficient, dimensionless and related to the fluid's Reynolds number and rheological parameters, 1; v is the fluid's velocity, m/s; and r_0 and r_1 are, respectively, the inner and outer diameters of the casing, m.

The heat balance equation for the casing wall is as follows:

$$\frac{2r_1(T_2 - T_1)}{R_1} - \frac{2r_0(T_1 - T_0)}{R_0} = \rho_1 C_1 \times (r_1^2 - r_0^2)\frac{\partial T_1}{\partial \tau} \tag{9}$$

where ρ_1 and C_1 are the density and specific heat capacity at constant pressure of the fracturing fluid, respectively, kg/m^3, kJ/(kg·°C); T_2 and T_1 are the temperature inside the casing and at the casing wall, respectively, °C; $R_1 = r_2 - r_1/2\lambda_2$, where λ_2 is the fluid's heat transfer coefficient, kJ/(m·min·°C); r_1 and r_2 are, respectively, the inner and outer diameters of the casing, m.

Assuming no heat transfer occurs in the circumferential direction, heat transfer occurs along the radial direction, and the control equation for temperature changes in the formation can be expressed as the following:

$$\frac{1}{\alpha_e}\frac{\partial T_e}{\partial \tau} = \frac{1}{e^{2\overline{r}}}\frac{\partial^2 T_e}{\partial \overline{r^2}} \tag{10}$$

where ρ_e is the density of the formation, kg/m^3; C is the specific heat capacity of the formation, kJ/(kg·°C); λ is the thermal conductivity of the formation, kJ/(m·°C); T_e is the temperature of the formation, °C; and r is the radius of the wellbore, m.

According to the forward equations, numerical calculation models are established, and the corresponding numerical solutions can be obtained by programming calculations. After combining with the actual fracture parameters, such as the flow rate of the multi-stage hydraulic fracturing process, wellhead pressure, and wellhead temperature, the alternating range of temperature and equivalent axial load for testing are found.

2.3.3. Experimental Loading Scheme for Casing Materials

According to the multistage hydraulic fracture parameters and theoretical calculation, the loading scheme of alternating thermal–mechanical coupling test for P110 casing is as follows:

The temperature loading scheme:

(1) Temperature alternating ranging is from 28 °C to 100 °C, and the frequency is every 30 min, as shown in Figure 5a.

(2) Temperature alternating ranging is from 28 °C to 150 °C, and the frequency is every 30 min, as shown in Figure 5b.

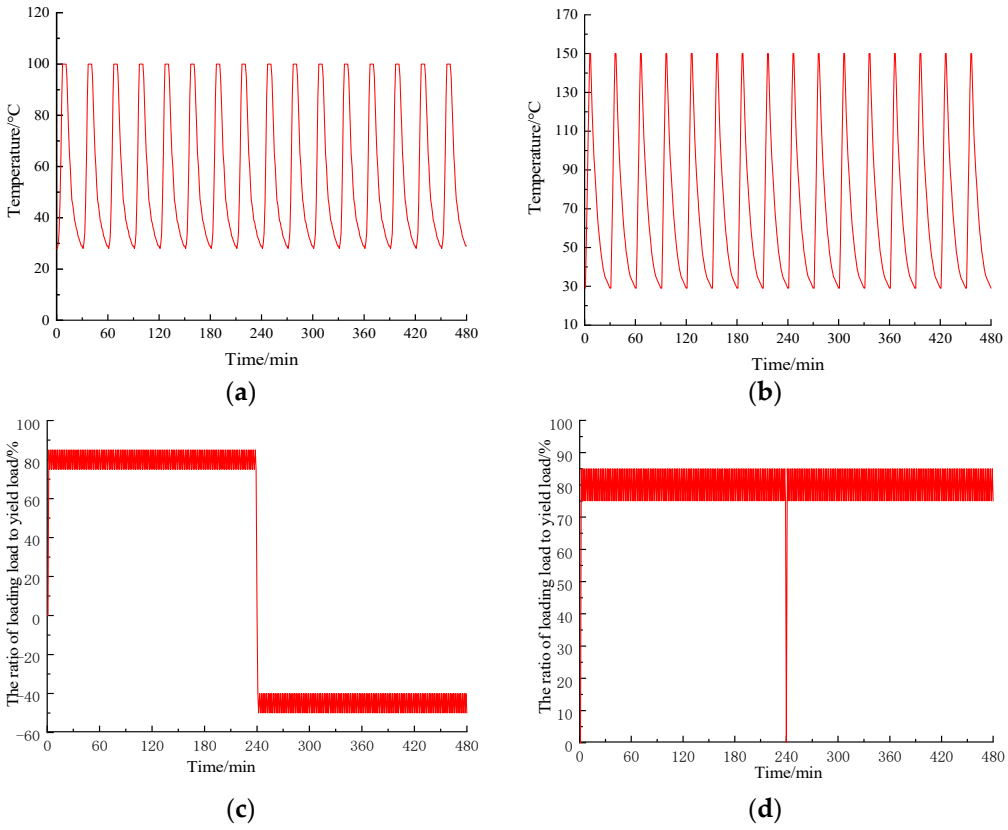

Figure 5. Load curve of alternating thermal–mechanical coupling test for casing material. (**a**) 28~100 °C temperature alternating curve. (**b**) 28~150 °C temperature alternating curve. (**c**) A single alternating T–C cycle curve. (**d**) A single alternating T–T cycle curve.

The coupling axial loading scheme:

(1) Alternating tension and compression (T–C) cycle test: A single cycle includes 4 h tensile load alternating, and 4 h compression load alternating, as shown in Figure 5c. The tensile load alternating range is 75–85% of the yield strength of P110 casing, while the compression load alternating range is 40% to 50% of the yield load. The alternating frequency is 1 Hz. The cycle number is 10, 20, 30, and 40 times, respectively.
(2) Alternating tension and tension (T–T) cycle test: A single cycle consists of 4 h tensile load alternating, then the load decreases to 0 kN, and followed by 4 h tensile load alternating again, as shown in Figure 5d. The tensile load alternating range is 75–85% of the yield strength of P110 casing. The alternating frequency is 1 Hz. The cycle number is 10, 20, 30, and 40 times, respectively.

And the specific parameters of alternating thermal–mechanical coupling test are shown in Table 2.

Table 2. Alternating thermal–mechanical coupling test parameters.

Temperature Alternating Range	Cycle Number under T–C Cycle Conditions	Cycle Number under T–T Cycle Conditions
28~100 °C	10 20 40	10 20 40
28~150 °C	10 30	10 30

3. Results and Discussion

3.1. Static Tensile Test Results of P110 Casing

Static tensile test under different temperature results of the P110 casing are shown in Table 3. Comparing with room temperature, the yield strength, ultimate strength, and elastic modulus at 100 °C are reduced by 10.56%, 0.53%, and 11.9%, respectively, while the yield strength, ultimate strength, and elastic modulus at 150 °C are reduced by 10.51%, 0.28%, and 3.5%, respectively. The decrease in yield strength at high temperature is the most significant.

Table 3. Static tensile test results of P110 casing.

Temperature/°C	Elastic Modulus/GPa	Yield Strength /MPa	Ultimate Strength /MPa
RT	208.87	939.58	1049.92
100 °C	183.81	840.35	1044.35
150 °C	201.55	840.78	1046.89

3.2. Strain Variation during Alternating Thermal–Mechanical Coupling Test

The strain curves of a single T–C cycle test under different alternating temperature conditions are illustrated in Figure 6. It is observed that the strain variation trend is consistent with the alternating frequency of temperature, but has a weak correlation with the axial load fluctuation during half of the cycle. And the strain alternating bandwidth is wider under low temperature than high temperature. Additionally, the strain increment is greater under temperature fluctuation within 28 °C to 150 °C than under temperature fluctuation within 28 °C to 100 °C. Therefore, the influence of temperature cycle on strain is greater than that of the load cycle in a half cycle.

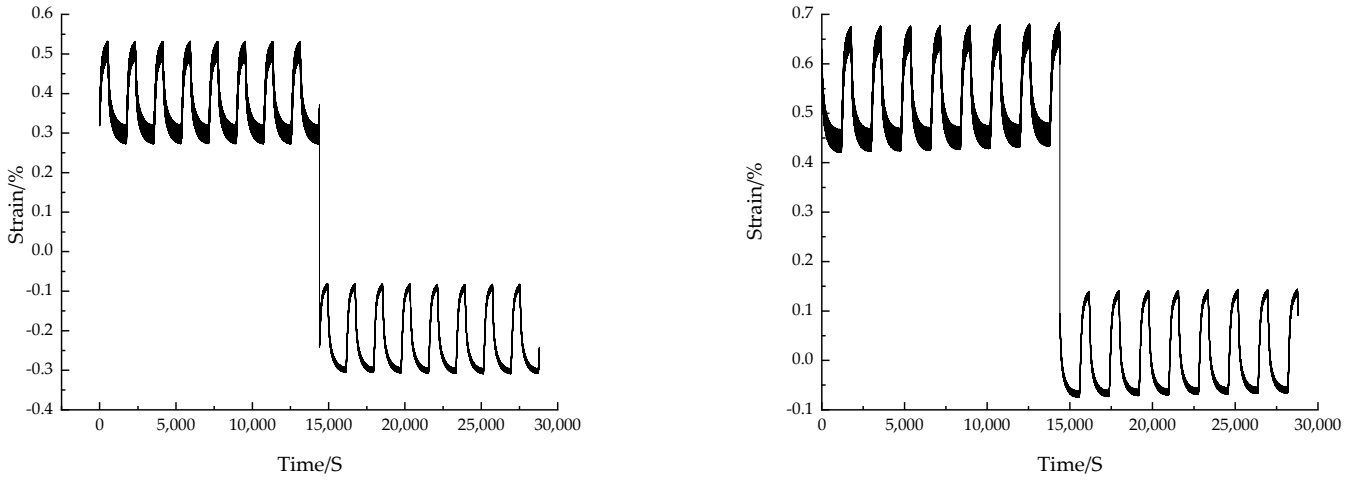

(**a**) (**b**)

Figure 6. The variation curve of axial strain of a single T–C cycle under different alternating temperature conditions. (**a**) Alternating temperature from 28 °C to 100 °C. (**b**) Alternating temperature from 28 °C to 150 °C.

In order to investigate the potential plastic deformation of samples long-term exposed to a coupled temperature and pressure alternating environment, the maximum strain data of every half cycle in a 10-time T–C coupling alternating load test is extracted, as shown in Figure 7. It is noticeable that as the number of large cycles increases, there is a corresponding rise in strain. The peak tensile strain increased from 0.32% to 0.37%, while the peak compressive strain increased from −0.23% to −0.18%, indicating an overall increase of 0.05% in both cases. This indicates that plastic deformation accumulation occurs in the specimen during the experiment.

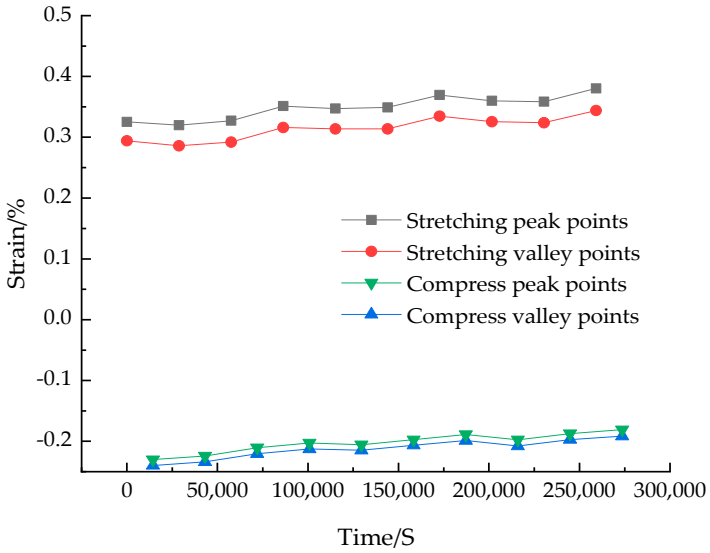

Figure 7. The variation curve of residual strain after 20 T–C cycles.

3.3. Yield Strength Variation after Alternating Thermal–Mechanical Coupling Test

Yield strength data is obtained from the tensile tests after different times of alternating thermal–mechanical coupling tests of casing materials provided by three representative manufacturers in China. The yield strength variation curves are depicted in Figure 8. The results exhibit good repeat-ability of three casing specimens.

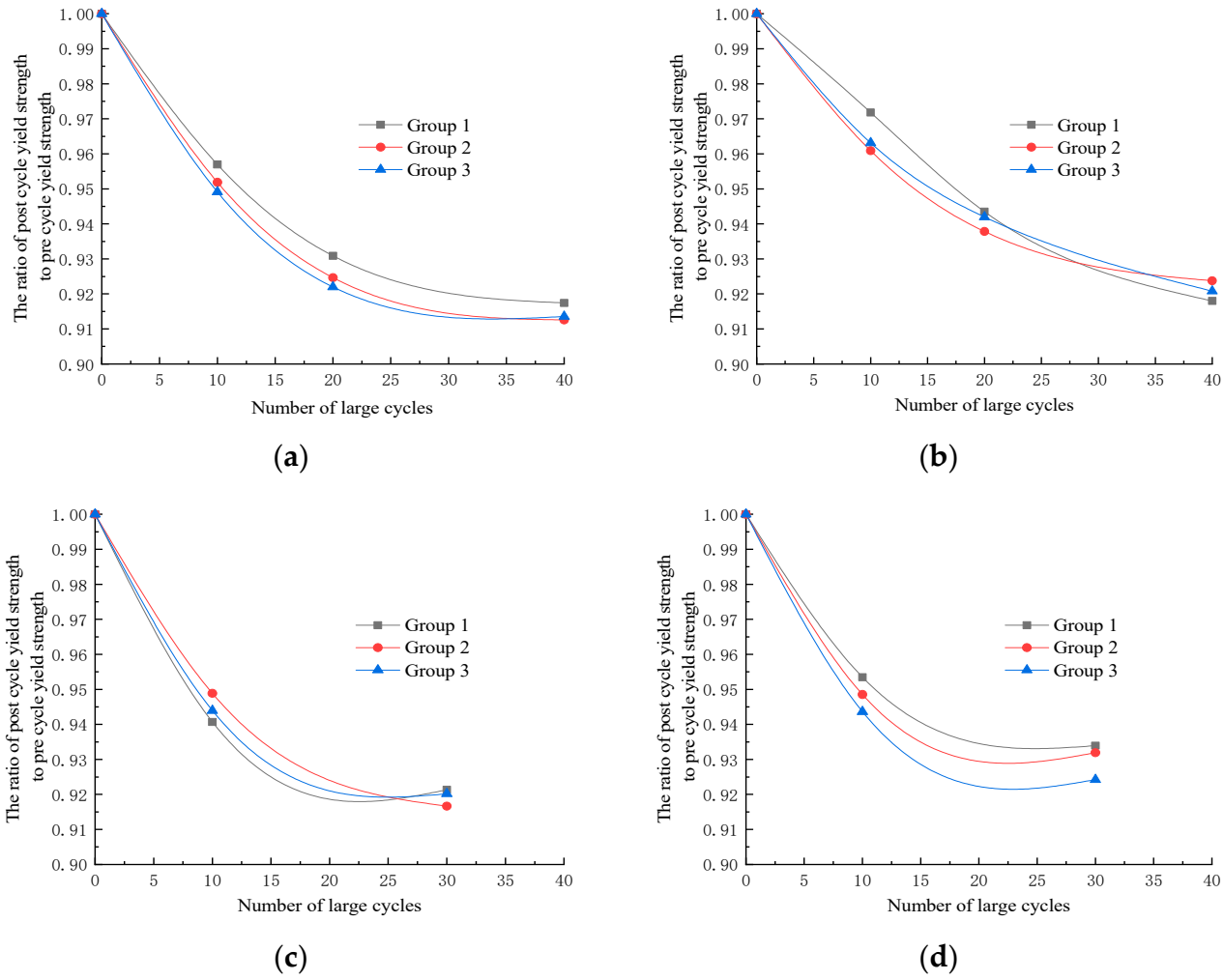

Figure 8. Yield strength variation curve of casing material after alternating thermal–mechanical coupling tests. (**a**) Yield strength variation curve of casing after T–T cycles with 28 °C to 100 °C temperature alternation. (**b**) Yield strength variation curve of casing after T–C cycles with 28 °C to 100 °C temperature alternation. (**c**) Yield strength variation curve of casing after T–T cycles with 28 °C to 150 °C temperature alternation. (**d**) Yield strength variation curve of casing after T–C cycles with 28 °C to 150 °C temperature alternation.

As the number of cycles increases, the yield strength decreases while the rate of decline slows down, and the whole curve shows an exponentially decreasing distribution pattern. Comparing Figures 8a and 8b, under the temperature alternation from 28 °C to 100 °C condition, T–T cycles lead to a greater reduction in yield strength than T–C cycles. After 10 cycles, T–T cycles corresponded to a 4.8% decrease in yield strength, while T–C cycles corresponded to a 3.5% decrease. After 20 cycles, T–T cycles resulted in a 7.4% decrease, while T–C cycles showed a 6.0% decrease in yield strength. After 40 cycles, T–T cycles lead to an 8.6% decrease, while T–C cycles lead to a 7.8% decrease in yield strength. Comparing Figures 8c and 8d, under a temperature variation from 28 °C to 150 °C, the pattern of yield strength variation is similar to that of 28 °C to 100 °C. Comparing Figures 8a and 8c, with the addition of T–T cycles, the decrease in yield strength of the casing material specimens is greater than that of the 28 °C to 100 °C temperature fluctuation. After 10 cycles and 30 cycles, the yield strength decreased by 5.5% and 8.2%, respectively. Comparing Figures 8b and 8d, under T–C cycle conditions, the yield strength decline is similar to that of T–T cycles.

3.4. Ultimate Strength Variation after Alternating Thermal–Mechanical Coupling Test

Figure 9 depicts the variation curves of the ultimate strength for casing material specimens after alternating thermal–mechanical coupling tests. As the number of cycles increases, the ultimate strength decreases while the rate of decline slows down, and the whole curve shows an exponentially decreasing distribution pattern. However, it is obvious that the ultimate strength decline rate of each sample has some difference due to being produced by different manufacturers.

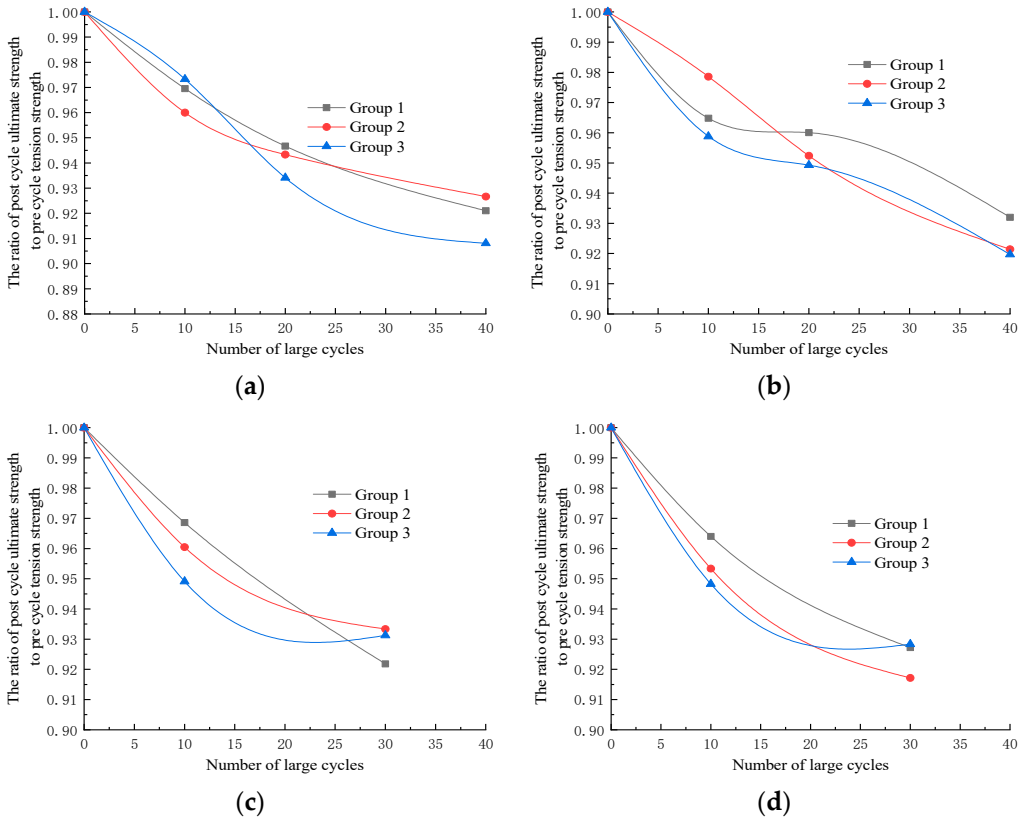

Figure 9. Ultimate strength variation curve of casing material after alternating thermal–mechanical coupling tests. (**a**) Ultimate strength variation curve of casing after T–T cycles with 28 °C to 100 °C temperature alternation. (**b**) Ultimate strength variation curve of casing after T–C cycles with 28 °C to 100 °C temperature alternation. (**c**) Ultimate strength variation curve of casing after T–T cycles with 28 °C to 150 °C temperature alternation. (**d**) Ultimate strength variation curve of casing after T–C cycles with 28 °C to 150 °C temperature alternation.

Comparing Figures 9a and 9b, under the temperature alternation from 28 °C to 100 °C condition, T–T cycles lead to a greater reduction in ultimate strength than T–C cycles. After 10 cycles, T–T cycles corresponded to a 3.6% decrease in ultimate strength, while T–C cycles corresponded to a 3.2% decrease. After 20 cycles, T–T cycles resulted in a 5.8% decrease, while T–C cycles showed a 4.7% decrease in ultimate strength. After 40 cycles, T–T cycles lead to a 7.5% decrease, while T–C cycles lead to a 6.9% decrease in ultimate strength. Comparing Figures 9c and 9d, under a temperature variation from 28 °C to 150 °C, the pattern of ultimate strength variation is similar to that of 28 °C to 100 °C. Comparing Figures 9a and 9c, with the addition of T–T cycles, the decrease in the ultimate strength of the casing material specimens is greater than that of the 28 °C to 100 °C temperature fluctuation. After 10 cycles and 30 cycles, the ultimate strength decreased by 4.0% and 6.9%, respectively. Comparing Figures 9b and 9d, under T–C cycle conditions, the ultimate strength decline is similar to that of T–T cycles.

3.5. The Effect of Low-Cycle Strain Fatigue and Alternating Temperature Aging

The 85% of yield strength at room temperature is 799 MPa, which is lower than the yield strength at 100 °C and 150 °C. Hence, the alternating axial load test belongs to low-cycle strain fatigue. It is well-known that strain fatigue can lead to plastic deformation accumulation, which causes dislocation proliferation and entanglement. These dislocation proliferations distribute around the local cementite. This kind of inhomogeneous dislocation distribution results in the increase in local strain energy. A large number of dislocation sources formed, which makes the grain more unstable and prone to deformation, thus reducing the strength of the material. Moreover, the dislocation plugging increases with the increase in the number of fatigue cycles. Therefore, low-cycle fatigue leads to a continuous decline in the residual strength of the material. On the other hand, the high-temperature aging leads to the reduction in free dislocation in the grain, which reduces the strengthening ability of a part of the grain boundary dislocation plugging during the deformation process, resulting in a decrease in strength.

Therefore, the alternating thermal–mechanical coupling is essentially the coupling effect of low-cycle strain fatigue and alternating high-temperature aging.

4. Prediction of Yield Strength of Casing after Alternating Thermal–Mechanical Coupling

The yield strength of the casing is the most critical mechanical parameter in engineering applications. In this section, the yield strength prediction method of the P110 casing after the alternating thermal–mechanical coupling test will be investigated and established according to the aforementioned test data.

The process of yield strength prediction is as follows:

(1) The average yield strength of different P110 casings under the same test conditions is obtained for the prediction model;
(2) Search for suitable yield strength prediction models for low-cycle strain fatigue;
(3) Search for suitable yield strength prediction models for alternating temperature aging;
(4) Analyze the reasonable correlation of the two models above; fit and build the yield strength prediction model of casing based on the alternating thermal–mechanical coupling test.

The decrease in residual strength caused by low-cycle fatigue is related to the relative fatigue cycle and strain amplitude. Analyzing the experimental data, it is found that the yield strength shows an exponential downward trend, but it comes to a steady state after a certain number of repetitions of the fatigue cycle. Therefore, we can use the allometric model [28] to fit the yield strength variation. The allometric model formula is shown as Equation (11):

$$\sigma_F = \sigma_0 - m\left(\frac{N_c}{N_f}\right)^P \tag{11}$$

where σ_F is the residual strength of the material after low-cycle fatigue damage, MPa; m is the deformation coefficient; P is the deformation index related to the load level; N_c stands for the current fatigue cycle; and N_f is the fatigue failure cycle.

Employing Formula (11), the corresponding fitting curve was obtained and shown in Figure 10. Meanwhile, the average values of yield strength calculated from Figure 8 are depicted as discrete points in Figure 10. The fitting result shows a good match with the experimental data, and the error is within 3.23%, and the yield strength fitting result of T–T fatigue is better than that of T–C cycles.

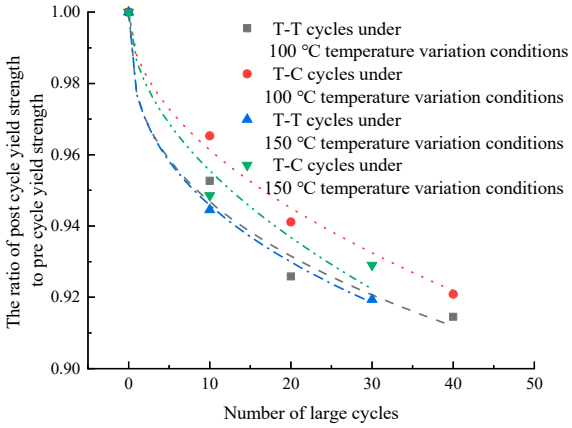

Figure 10. Fitting curve of yield strength after low-cycle strain fatigue.

The decline of residual strength caused by alternating high-temperature aging is related to the aging time. The experimental yield strength variation trend is consistent with the ExpDec model [28], and ExpDec model is depicted as Equation (12):

$$\sigma_{AT} = \sigma_0 - Te^{t/t_0} \tag{12}$$

where σ_{AT} is the residual strength after alternating temperature aging; σ_0 is the material's initial yield strength, Mpa; T is the temperature coefficient; and t_0 is the temperature index.

The alternating mechanical load and temperature load exhibit a significant mutual interaction mechanism. Hence, their coupling effect on yield strength involves low-cycle strain fatigue and alternating temperature age. Based on Equations (11) and (12), the yield strength after the cycling prediction model is conducted is shown as Equation (13):

$$\frac{\sigma_{FT}}{\sigma_0} = 1 - Ke^{t/t_0}N_c^P \tag{13}$$

where σ_{FT} is the yield strength of the casing material after the alternating thermal–mechanical coupling load, Mpa; and K is a constant related to temperature coefficient T, deformation coefficient P, fatigue failure cycle N_f, and the material's initial yield strength σ_0.

The fitting result is illustrated in Figure 11, and the results show that the fitting results match well with the experimental data. It is observed that the fitting effect for the T–T cycle data is better than that of T–C cycles, with an error of 2.89%. Comparing the experimental data, shown as discrete points, and the fitting curve shown in Figure 11, Formula (13) is considered to be effective in the yield strength prediction after alternating thermal–mechanical coupling loads.

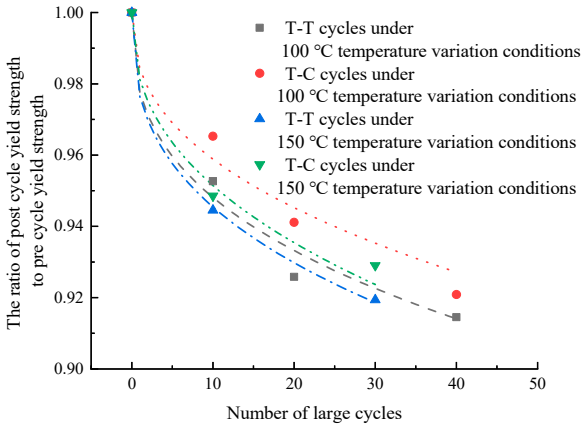

Figure 11. Fitting curve of yield strength after alternating thermal–mechanical coupling tests.

5. Conclusions

(1) A theoretical model related to the alternating temperature and pressure of the casing during hydraulic fracturing was established. The temperature and equivalent axial load variation range were calculated by the theoretical model, which provides the experimental loading parameters for alternating thermal–mechanical coupling tests of the P110 casing.

(2) The alternating thermal–mechanical coupling loads significantly lead to a reduction in the yield strength, ultimate strength, and elastic modulus of the P110 casing material. The yield strength and ultimate strength show an initial rapid decline with the increase in the alternating cycles of axial load and temperature, followed by a gradual decrease.

(3) T–T load cycles induce greater reductions in both yield strength and ultimate strength than that of T–C load cycles. After 40 cycles with the alternating temperature from 28 °C to 100 °C, T–T cycles led to a 0.8% reduction in yield strength and a 0.7% reduction in ultimate strength compared to T–C cycles. Under 30 cycles with the alternating temperature from 28 °C to 150 °C, T–T cycles resulted in a 0.2% reduction in yield strength and a 0.3% reduction in ultimate strength compared to T–C cycles.

(4) The yield strength of P110 casing materials under the alternating thermal–mechanical coupling loads exhibits a coupled impact of low-cycle strain fatigue and alternating temperature aging. The yield strength of the P110 casing material after alternating thermal–mechanical coupling test decreases following a $Ke^{t/t_0}N_c^P$ pattern.

Author Contributions: C.L., S.Y. and J.W. conceived and designed the experiments; C.L., X.Z. and H.Z. performed the experiments; C.L., X.Z. and L.H. analyzed the data; H.Z. and Y.Q. contributed analysis tools; C.L. wrote the paper. All authors have read and agreed to the published version of the manuscript.

Funding: This research was funded by National Key R&D Program of China, grant number 2023YFB3711700, National Natural Science Foundation of China, grant number 52104004, and Scientific Research and Technology Development of CNPC 2021DJ4403.

Data Availability Statement: Data are contained within the article.

Conflicts of Interest: Author Yue Qi was employed by the company Drilling Engineering Technology Research Institute of Daqing Drilling Engineering Company. The remaining authors declare that the research was conducted in the absence of any commercial or financial relationships that could be construed as a potential conflict of interest.

References

1. Jiao, F. Re-recognition of "unconventional" in unconventional oil and gas. *Pet. Explor. Dev.* **2019**, *46*, 847–855. [CrossRef]
2. Song, Y.; Li, Z.; Jiang, Z.; Luo, Q.; Liu, D.; Gao, Z. Progress and development trend of unconventional oil and gas geological research. *Pet. Explor. Dev.* **2017**, *44*, 675–685. [CrossRef]
3. Liu, N.; Zhang, Z.; Zou, Y.; Ma, X.; Zhang, Y. Propagation law of hydraulic fractures during multi-staged horizontal well fracturing in a tight reservoir. *Pet. Explor. Dev.* **2018**, *45*, 1059–1068. [CrossRef]
4. Chen, Z.; Shi, L.; Xiang, D. Mechanism of casing deformation in the Changning–Weiyuan national shale gas project demonstration area and countermeasures. *Nat. Gas Ind.* **2016**, *36*, 70–75.
5. Zou, C.; Yang, Z.; Zhu, R.; Zhang, G.; Hou, L.; Wu, S.; Tao, S.; Yuan, X.; Dong, D.; Wang, Y.; et al. Progress in China's Unconventional Oil & Gas Exploration and Development and Theoretical Technologies. *Acta Geol. Sin.-Engl. Ed.* **2015**, *89*, 938–971.
6. Zhao, C. Investigation on Failure Mechanism and Test of Casing Deformation in Shale Gas Wells during Multi-Fracturing. Ph.D. Thesis, China University of Petroleum (Beijing), Beijing, China, 2021.
7. Khan, R.A.; Ahmad, S. Nonlinear dynamic and bilinear fatigue reliability analyses of marine risers in deep offshore fields. *Ships Offshore Struct.* **2018**, *13*, 10–17. [CrossRef]
8. Liu, X.; Qiu, N.; Wang, X.; Chang, Y.; Chen, G. Analysis on fatigue failure of deep water drilling riser based on fracture mechanics. *Pet. Eng. Constr.* **2020**, *46* (Suppl. S1), 138–144.
9. Xiao, N.; Hui, W.; Zhang, Y.; Zhao, X.; Chen, Y.; Dong, H. High-Cycle Fatigue Behavior of Vacuum-Carburized 20Cr2Ni4 Steel with Different Case Depths. *J. Mater. Eng. Perform.* **2019**, *28*, 3413–3422. [CrossRef]
10. Teodoriu, C.; Ulmanu, V.; Badicioiu, M. Casing fatigue life prediction using local stress concept: Theoretical and experimental results. In Proceedings of the SPE Western Regional Meeting, Bakersfield, CA, USA, 31 March–2 April 2008.

11. Zhou, K.; Hou, J.; Yu, B.; Du, Q.; Liu, Y. Production analysis of sequential multi-well cyclic steam stimulation in heterogeneous heavy oil reservoir. *Int. J. Oil Gas Coal Technol.* **2017**, *16*, 311–328. [CrossRef]
12. Maruyama, K.; Tsuru, E.; Ogasawara, M.; Inoue, Y.; Peters, E.J. An experimental study of casing performance under thermal cycling conditions. *SPE Drill. Eng.* **1990**, *5*, 156–164. [CrossRef]
13. Hsu, S.Y.; Searles, K.H.; Liang, Y.; Wang, L.; Dale, B.A.; Grueschow, E.R.; Spuskanyuk, A.; Templeton, E.L.; Smith, R.J.; Lemoing, D.R. Casing Integrity Study for Heavy-Oil Production in Cold Lake. In Proceedings of the SPE Annual Technical Conference and Exhibition, Florence, Italy, 20–22 September 2010.
14. Plácido, J.C.; Ademar, P., Jr.; Paulo, L.A.; Pasqualino, I.P.; Estefen, S.F. Stress-Analysis of Casing String Submitted to Cyclic Steam Injection. In Proceedings of the Latin American and Caribbean Petroleum Engineering Conference, Rio de Janeiro, Brazil, 30 August–3 September 1997.
15. Kaiser, T.M.V. Post-Yield Material Characterization for Thermal Well Design. In Proceedings of the SPE International Thermal Operations and Heavy Oil Symposium, Calgary, AB, Canada, 1–3 November 2005.
16. Gan, Q. Casing Damage Mechanism of Thermal Recovery Wells. Master's Thesis, Southwest Petroleum University, Chengdu, China, 2017.
17. Yin, F.; Han, L.; Yang, S.; Deng, Y.; He, Y.; Wu, X. Casing deformation from fracture slip in hydraulic fracturing. *J. Pet. Sci. Eng.* **2018**, *166*, 235–241. [CrossRef]
18. Yin, H.; Zhang, Y. A quantitative evaluation method for the effect of temperature on casing collapsing strength—A case study of large-scale hydraulic fracturing in shale gas horizontal wells. *Nat. Gas Ind.* **2016**, *36*, 73–77.
19. Tian, Z.; Shi, L.; Qiao, L. Research of and countermeasure for wellbore integrity of shale gas horizontal well. *Nat. Gas Ind.* **2015**, *35*, 70–76.
20. Liu, Z.; Samuel, R.; Gonzales, A.; Kang, Y. Analysis of casing fatigue failure during multistage fracturing operations. In Proceedings of the Abu Dhabi International Petroleum Exhibition & Conference, Abu Dhabi, UAE, 12–15 November 2018.
21. An, F.; Zhang, F.; Yi, H.; Zhang, S. Effects of alternating stress on casing damage mechanism. *Coal Geol. Explor.* **2021**, *49*, 143–150.
22. Wu, R.; Jiang, D.; Ren, L. A research on life forecast model of high pressure and tempreture gas well pipe. *Manuf. Autom.* **2011**, *33*, 133–134.
23. Mou, Y.; Lian, Z.; Lin, T.; Zhang, Q.; Liu, Y. Study on fatigue of tubing joint thread induced by vibration in HTHP ultradeep wells. *J. Press. Vessel. Technol.* **2020**, *142*, 031502. [CrossRef]
24. Wang, J.; Lu, C.; He, H.; Sun, J.; Wu, X.; Li, F. Selection and Evaluation of Pipe String in Underground Gas Storage with Gas Reservoirs. *Pet. Tubul. Goods Instrum.* **2019**, *5*, 26–29.
25. Wang, J.; Feng, Y.; Yan, X.; Lin, K.; Lu, C. Experimental research on material properties of High-grade steel casing at high temperature. In Proceedings of the 2010 Cross Strait Material Destruction/Fracture Academic Conference, Taiwan, China, 21 September 2010.
26. *GB/T 43231-2023*; Petroleum and Natural Gas Industries—Selection and Adaptability Evaluation of Casing for Shale Oil and Gas Wells. Standardization Administration of China: Beijing, China, 2023.
27. *T/CSTM 00397-2023*; Testing and Evaluation Method of Casing String for Complex Fracturing. CSTM: Beijing, China, 2023.
28. Yang, J.; Ma, H.; Wang, H.; Hu, Y.; Yang, K.; Zhou, X.; Wei, W. Residual Strength of P110H Casing Steel under High Temperature Service Condition. *Hot Work. Technol.* **2022**, *51*, 142–145.